Particle & Particle Systems Characterization
www.particle-journal.com

Observation of Undamped 3D Brownian Motion of Nanoparticles Using Liquid-Cell Scanning Transmission Electron Microscopy

Tom A. J. Welling, Sina Sadighikia, Kanako Watanabe, Albert Grau-Carbonell, Maarten Bransen, Daisuke Nagao, Alfons van Blaaderen, and Marijn A. van Huis**

In theory, liquid-cell (scanning) transmission electron microscopy (LC(S)TEM) is the ideal method to measure 3D diffusion of nanoparticles (NPs) on a single particle level, beyond the capabilities of optical methods. However, particle diffusion experiments have been especially hard to explain in LC(S)TEM as the observed motion thus far has been slower than theoretical predictions by 3–8 orders of magnitude due to electron beam effects. Here, direct experimental evidence of undamped diffusion for two systems is shown; charge-neutral 77 nm gold nanoparticles in glycerol and negatively charged 350 nm titania particles in glycerol carbonate. The high viscosities of the used media and a low electron dose rate allow observation of Brownian motion that is not significantly altered by the electron beam. The resulting diffusion coefficient agrees excellently with a theoretical value assuming free diffusion. It is confirmed that the particles are also moving in the direction parallel to the electron beam by simulating STEM images using Monte Carlo simulations. Simulations and experiments show blurring of the particles when these move out of focus. These results make clear that direct observation of 3D diffusion of NPs is possible, which is of critical importance for the study of interparticle interactions or in situ colloidal self-assembly using LC(S)TEM.

1. Introduction

Direct visualization of dynamic processes of sub-micron particles in liquids via microscopy techniques has helped researchers acquire many insights in interesting topics such as interparticle interactions and colloidal self-assembly.[1–3] Liquid-cell (scanning) transmission electron microscopy[4,5] (LC(S)TEM) has recently emerged as a powerful tool to observe dynamic processes of nanoparticles (NPs) in liquid with nanometer spatial resolution.[6–29] However, the electron beam significantly influenced the observed phenomena in many cases. So far, strongly slowed down diffusion of NPs was observed in LC(S)TEM studies.[6–29] Possible explanations for this phenomenon, apart from trivial difficulties such as the imaging system not being fast enough to image free Brownian motion, include hydrodynamic slowing down near the window's surface,[10,16] a highly viscous ordered liquid layer near the windows,[10,15] and strong (sometimes beam-induced) interactions with the liquid-cell windows.[6,10,15,16,18] Observing 3D Brownian motion in the electron microscope that is not significantly altered by the electron beam and/or the presence of the windows would open the way for many experiments, including studies on colloidal self-assembly of NP dispersions.[30] The objective of this work is to find conditions and identify key experimental parameters for which 3D Brownian motion is observable in LC(S)TEM.

In this study, we combine a low dose scanning transmission electron microscopy (STEM) technique with viscous liquid media having a high dielectric constant to observe bulk diffusion of gold NPs and titania particles in LC(S)TEM. The significantly faster diffusion of particles in comparison to many previous liquid-cell electron microscopy studies that we report on in this work underlines the importance of choosing a suitable electron microscopy imaging technique, electron dose rate and solvent in order to study dynamic processes in LC(S)TEM without artefacts.

2. Results and Discussion

For this work, we studied two different systems. One with bigger particles in a less viscous solvent and one with smaller particles in a more viscous solvent. The bigger particles serve as a first check whether free diffusion is at all possible within the

T. A. J. Welling, S. Sadighikia, A. Grau-Carbonell, M. Bransen, Prof. A. van Blaaderen, Dr. M. A. van Huis
Soft Condensed Matter
Debye Institute for Nanomaterials Science
Utrecht University
Princetonplein 5, Utrecht 3584 CC, The Netherlands
E-mail: A.vanBlaaderen@uu.nl; M.A.vanHuis@uu.nl
Dr. K. Watanabe, Prof. D. Nagao
Department of Chemical Engineering
Tohoku University
6-6-07 Aoba, Aramaki-aza, Aoba-ku, Sendai 980-8579, Japan
The ORCID identification number(s) for the author(s) of this article can be found under https://doi.org/10.1002/ppsc.202000003.

DOI: 10.1002/ppsc.202000003

electron microscope. The smaller particles allow us to explore the feasibility for 3D diffusion experiments for NPs smaller than 100 nm as these are small enough to change their position away from focus conditions.

First, glycerol carbonate (GC) was used as a solvent wherein spherical 350 nm sized TiO_2 particles were dispersed. These particles were synthesized via the method by Mine et al.[31] and have a polydispersity of 10%. GC is a solvent with a high viscosity ($\eta = 0.147$ Pa s) and high dielectric constant ($\varepsilon_r = 111.5$).[32] The high dielectric constant is believed to decrease the induced electric fields due to STEM irradiation.[33] Moreover, because of the strong resemblance of properties of GC to water, it is proposed as a low vapor pressure green alternative in cases where for instance a low vapor pressure/high boiling point is important.[34,35] In combination with a low electron dose rate (0.6–2.4 e^- nm^{-2} s^{-1} in this study), the influence of the electron beam can be minimized. This dose rate is at least one order of magnitude lower than previous LC(S)TEM NP diffusion studies. It has been shown theoretically[36] that the spatial resolution scales with the electron dose d as res $\propto d^{-1/4}$. This indicates that even a reduction of the electron dose rate by 3 orders of magnitude only decreases the spatial resolution by a factor of 5, which indicates that extremely low dose rates are useful for many experiments. Moreover, in case the particle density is not too high, the actual accuracy of the spatial coordinates of the particles can be significantly higher than the resolution.[37]

The dispersion was enclosed between two silicon microchips with 50-nm-thick electron-transparent amorphous silicon nitride (SiN_x) windows (**Figure 1**a). The chips are loaded on a dedicated TEM holder and inserted in the electron microscope. Multiple annular dark-field (ADF) STEM videos of the observed particle diffusion can be found in Supporting Information. Figure 1 shows several frames of raw ADF-STEM footage showing individual particle diffusion, along with their complete trajectory (details in Supporting Information). The trajectories of 14 particles (observations longer than 100 s) were obtained and the mean squared displacement (MSD) is shown in **Figure 2**a.

The ensemble averaged MSD was determined by making use of lag times[38–40]:

$$<(\vec{r}(\Delta+n\tau)-\vec{r}(n\tau))^2> = \frac{1}{N_p}\sum_{i=1}^{N_p}\frac{1}{N\tau-\Delta}\sum_{n=1}^{N-\Delta/\tau}(\vec{r}_i(\Delta+n\tau)-\vec{r}_i(n\tau))^2 \quad (1)$$

Here $\vec{r}_i(n)$ is the position of particle i in frame n, N the total amount of frames, τ the duration of 1 frame and N_p the total amount of particles. The lag time Δ replaces the function of time in the more straightforward MSD analysis. The value for D was then determined by a weighted least-square fit to the obtained ensemble averaged MSD (Figure 2b) with a function $f = D/4 \times \Delta$. The fit to the ensemble averaged MSD yielded a diffusion coefficient $D = (12.8 \pm 0.2) \times 10^{-3}\,\mu m^2\,s^{-1}$. Next, we calculated the diffusion coefficient of 350 nm titania particles in pure GC at 25 °C via the Stokes–Einstein relation, thus assuming free 3D diffusion:

$$D = \frac{k_B T}{6\pi\eta a} \quad (2)$$

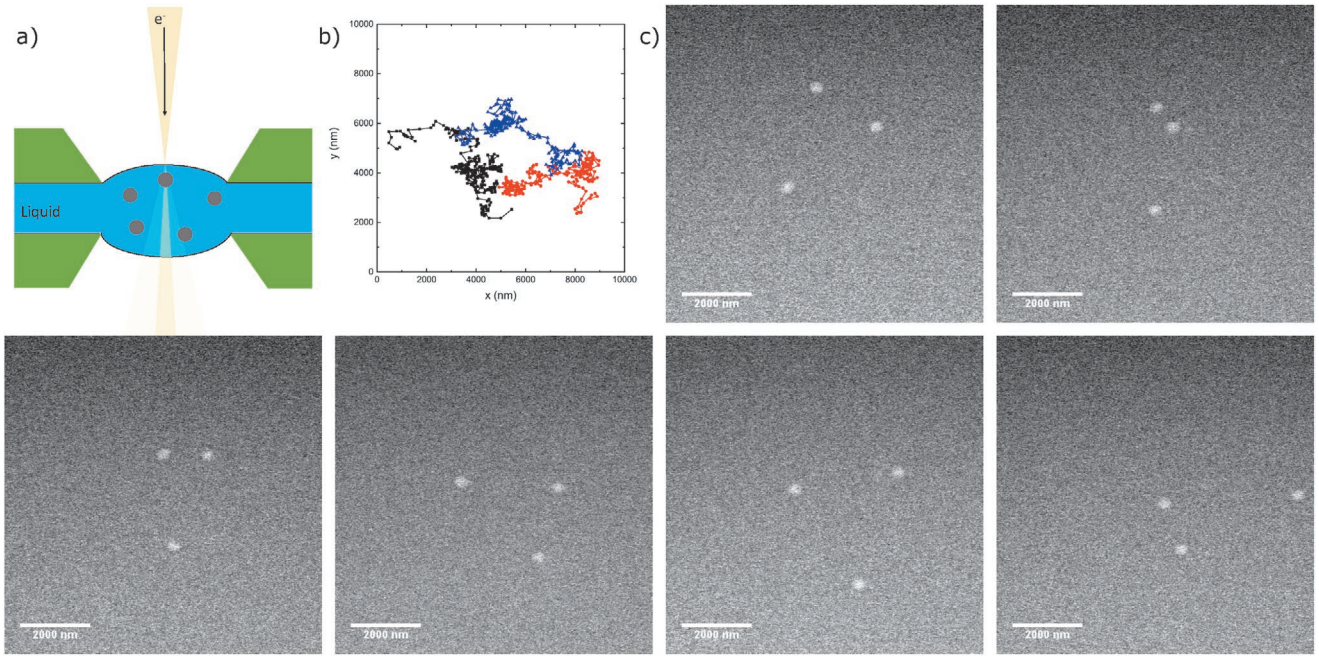

Figure 1. Motion of 350 nm titania particles within the liquid-cell. a) Schematic of the liquid-cell configuration in the microscope. A focused STEM beam probes the sample, which consists of titania particles dispersed in glycerol carbonate in between SiN_x windows. b) Full trajectories of the particles shown in the panels in c and in Movie S1, Supporting Information, during 100 s. c) Stills of an ADF-STEM recording showing particle movement in time. The frame time was 0.5 s and frames were acquired continuously (no delay between frames). The frame dimensions are 512 × 512 pixels with a pixel size of 17.5 nm. The electron dose rate was 2 e^- nm^{-2} s^{-1}.

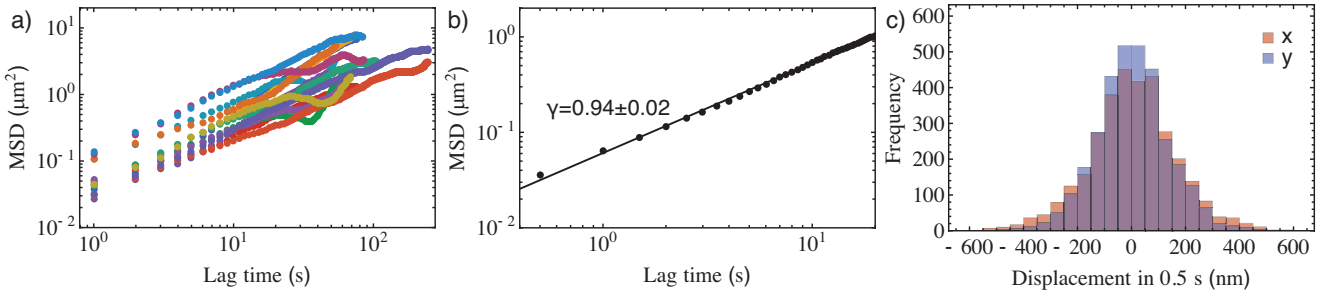

Figure 2. The MSD of 350 nm titania particles in the liquid-cell. a) Single particle trajectories for 14 particles that were tracked for at least 100 s. The frame time was 0.2 or 0.5 s and the frames were acquired continuously. The frames for various videos were with dimenions of 256 × 256 or 512 × 512 pixels. The pixel size for various videos was between 17.5 and 49.5 nm. b) MSD averaged over all the single particle trajectories from (a). The slope of the averaged MSD is 0.94 ± 0.02, indicating slightly subdiffusive behavior. c) Displacement histograms of the steps taken by the particles between frames in the x- and y-directions.

where k_B is the Boltzmann constant, T the absolute temperature, η the dynamic viscosity and a is the radius of the particles. The calculated diffusion coefficient of $D = 11.5 \times 10^{-3}\,\mu m^2\,s^{-1}$ agrees relatively well with the experimentally obtained diffusion coefficient. The deviation from the experimental value obtained from the ensemble averaged MSD can be explained due to a slight deviation in temperature or liquid composition leading to a significant change in viscosity.

It is likely that the entrapment of the liquid between windows has an influence on the motion of the particles. We analyzed the slope of the MSD in a logarithmic plot (Figure 2b). The obtained MSD was fitted to a function $f = C\Delta^{\gamma}$, with C a fitting constant. If the value of γ is 1, the motion is truly Brownian, if it is less than 1 it indicates subdiffusive behavior, while it shows superdiffusive behavior for $\gamma > 1$.

The slope of the MSD is 0.94 ± 0.02 indicating slightly subdiffusive behavior. The small deviation could be explained by the influence of the windows. We calculated the liquid thickness with the method reported by Verch et al.[15] and found that the liquid thickness is 2.3 ± 0.7 μm. It is likely that, within the time frame of our observations, particles notice the presence of the static hindrance of the windows, leading to slightly subdiffusive behavior. The much more pronounced subdiffusive behavior often found in LC(S)TEM experiments was not found in this study.[41] Additional evidence for Brownian diffusion is shown in Figure 2, where the displacements of particles per frame is normally distributed.

As the liquid layer is less than 10 times the particle diameter in thickness, some hydrodynamic slowing down of the particles is expected. For a particle size of 350 nm in liquid between two parallel plates 2.3 μm apart, particles are expected to slow down by approximately 15% when moving parallel to the two plates.[42] However, due to insufficient knowledge on the exact temperature and liquid composition, it could not be accurately tested. It could however, lead to differences in MSDs of individual particles. We stress that hydrodynamic slowing down should always be considered in future dynamic liquid-cell experiments, especially for much lower liquid thicknesses.

To investigate whether the particle also move in the direction parallel to the STEM probe, we simulated ADF-STEM images using the experimental conditions for a 350 nm titania particle at various heights in the liquid-cell, using the CASINO software.[43–45] **Figure 3** shows the simulated ADF-STEM images for a titania particle at the top, middle and bottom of the liquid-cell. No obvious difference is observed, because at 350 nm size the particle is too large to move out of focus or be significantly influenced by beam broadening effects. This agrees with experiments where we do not see any change in focus conditions for the freely diffusing particles between frames. Since no hopping motion is observed and the experimental diffusion coefficient is close to that expected for free diffusion, it is likely that the particle is also diffusing in the third dimension. Below we will demonstrate that this is the case for smaller NPs.

Many LC(S)TEM studies also show a significant influence of the electron beam on the acquired data. Effects like radiolysis,[46] bubble formation,[46] momentum transfer,[19] and increased temperature[19] have all been analyzed (details in Supporting Information). However, the charged titania particles we believe the reduction of charging and electric field effects is the main reason that free diffusion is observed. Woehl et al. have previously explained the repulsion of titania particles from the window by discussing electric fields.[17] However, their electron dose rate was 2–3 orders of magnitude higher than the dose rates used in this study. In the modeling of beam-induced electric fields by Jiang, positive charges concentrate within the probed region of a focused STEM probe, leading to electric fields that are cylindrically symmetric around the probed region with their strength decaying away from the probe,[47] via[48]

$$|E| = \frac{\rho}{2\pi\varepsilon_0\varepsilon_r R} \tag{3}$$

Here ρ is the induced charge density, which depends on the used electron dose rate and the width of the STEM probe, ϵ_r the relative dielectric constant of the medium and R the distance from the STEM probe. The electric field arises due to emission of secondary and Auger electrons, which are not immediately neutralized, leaving behind a positively charged region.[47] In liquid, like in our experiment, the electric field will be screened by ions present in the solution. Since the titania particles are negatively charged and the entire field of view is quickly scanned by the probe, an effect of the electric field would be seen by the titania particles not being able to leave the field of view. However, during our observations 51 titania particles leave and 44 titania particles enter the field of view (Supporting Information), indicating a negligible effect of the induced electric

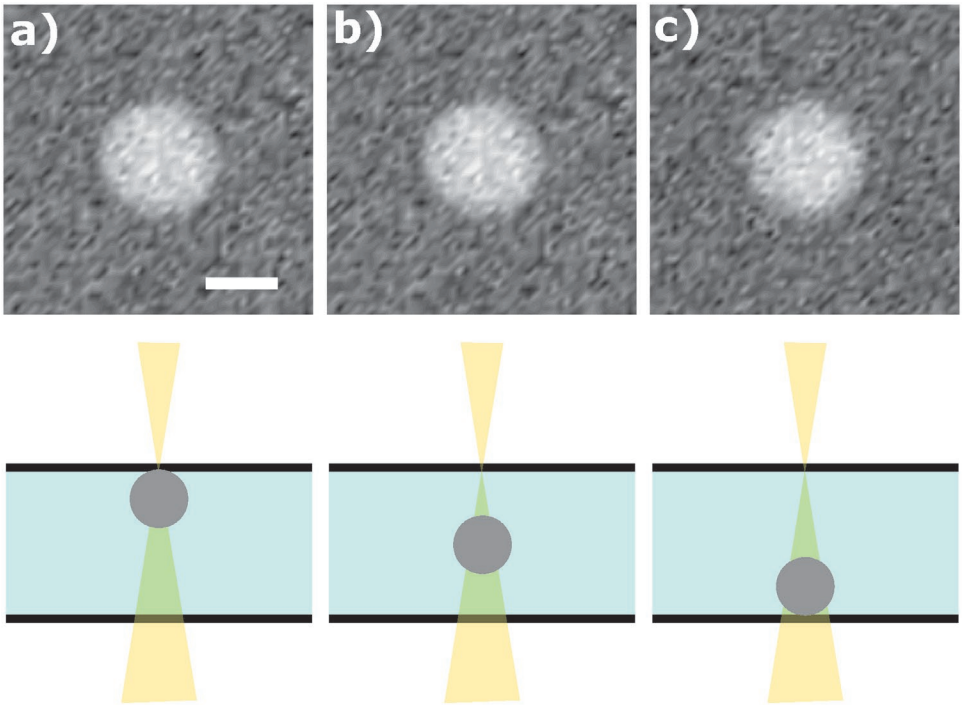

Figure 3. Simulated ADF-STEM images of a 350 nm titania particle using the software CASINO. The particle was positioned at different heights in the liquid-cell; a) on the top window, b) in the middle of the cell, and c) on the bottom window. The liquid thickness used was 2.3 μm. The input parameters for the Monte Carlo simulations were the same as used in the experiment for Movie S1, Supporting Information. The pixel size was 17.5 nm, the pixel dwell time was 1.9 μs and the electron dose rate was 2 e^{-} nm^{-2} s^{-1}. The focal point was on the top window and the semi-convergence angle α of the electron probe was 10 mrad. The scalebar is 200 nm.

fields or effects like thermophoresis with the used electron dose rates and solvent. We hypothesize that the low electron dose rate results in a lower induced charge density ρ, which in addition is screened by charged species and their conductivity in the strongly polar solvent. Using GC as a liquid is therefore important because of its high ϵ_r. A high dielectric constant liquid screens the charges that are induced by the beam on the windows. The addition of salt would help the screening of charges even more.

LC(S)TEM is primarily useful to observe NPs in a liquid environment in real time beyond the capability of optical methods. Ideally, we would have imaged NPs in glycerol carbonate as in that medium less bubble formation occurs than in glycerol. However, as the diffusion coefficient of a particle scales with the inverse of their radius, NPs would move too fast in glycerol carbonate. We thus decided to use glycerol as a liquid medium for charge-neutral 77 nm gold NPs with polyethylene glycol (PEG) ligands, synthesized via a slightly modified procedure based on the protocol of Hanske et al.[49] (Supporting Information). Glycerol has a viscosity of η = 0.9 Pa s at 25 °C, which is an order of magnitude higher than that of glycerol carbonate, and has a dielectric constant of 42.5. We dispersed the gold NPs coated with PEG in a mixture of 98 vol% of glycerol and 2 vol% of water. **Figure 4** shows various frames of Movie S4, Supporting Information, in which gold particles are diffusing within the liquid-cell. In any given frame, distinct particles are clearly blurred to various extents, indicating they are at different heights within the liquid-cell.

In order to determine whether the motion is anomalous due to electron beam effects,[41] we first analyze the tracks obtained from Movie S4, Supporting Information (**Figure 5**a). Figure 5b shows the histogram of displacements between two consecutive frames over all frames of Movie S4, Supporting Information. We observe that on average the displacements in x are slightly higher than the displacements in y, which may be related to the scanning direction. The MSDs for the individual particles are shown in Figure 5c, whereas an ensemble averaged MSD is shown in Figure 5d. The slope of the ensemble averaged MSD in a log–log plot is 0.98 ± 0.01 indicating Brownian diffusion. The diffusion coefficient obtained from the ensemble averaged MSD is $D = (8.8 \pm 0.1) \times 10^{-3}\,\mu m^2\,s^{-1}$. This is in reasonable agreement with the diffusion coefficient calculated via Equation (2) for 77 nm Au NPs with PEG ligands (hydrodynamic radius a = 42 nm) in 98/2 vol% glycerol/water at 25 °C (viscosity $\eta = 0.65$ Pa s), which is $D = 8.0 \times 10^{-3}\,\mu m^2\,s^{-1}$. A slight change in either temperature or water content could explain the discrepancy between the experimental and theoretical result, which is not unreasonable since both are hard to control precisely.

Next, we focus our attention to the motion of the particles in the z-direction. **Figure 6** shows the same particle at different times in Movie S4, Supporting Information. In a time span of 100 s it moves from being in focus near the top of the liquid-cell to blurry near the bottom of the cell and then moves back to the top.

To show that a different z position within the liquid-cell can indeed lead to a blurring of the particle as shown in Figure 6 (and Figure S8, Supporting Information), we used

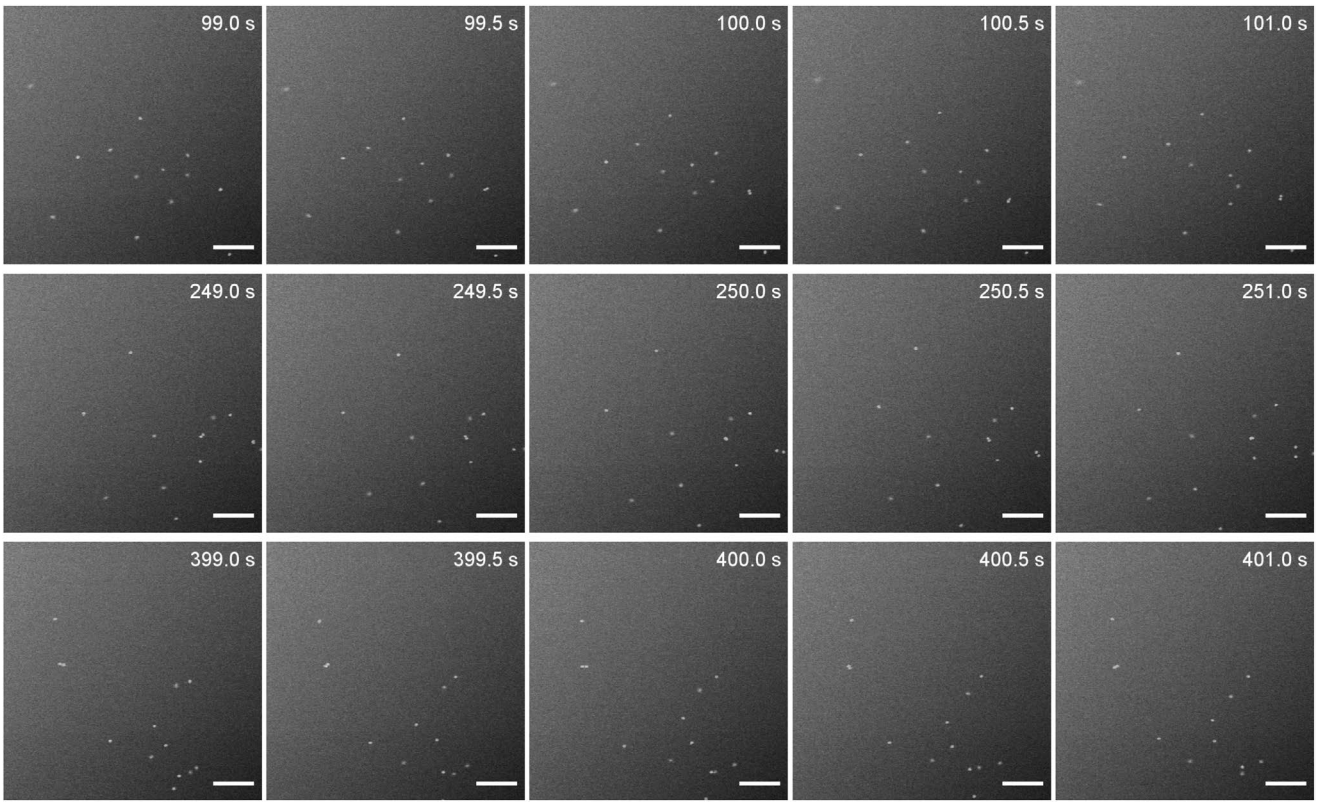

Figure 4. Motion of 77 nm gold NPs within the liquid-cell. The frame time was 0.5 s and frames were acquired continuously (no time between frames). The frame was 512 × 512 pixels with a pixel size of 12.2 nm. The electron dose rate was 9 e^{-} nm^{-2} s^{-1}. Individual frames taken from Movie S4, Supporting Information. The scalebar is 1 μm.

the Monte Carlo software CASINO[43–45] to simulate ADF-STEM images of the gold NPs as well. **Figure 7** shows the simulated ADF-STEM images of a 77 nm gold NP at various heights z within the liquid-cell. The simulations confirm that the image of the gold NP becomes blurry as it moves closer to the bottom of the cell. This could be due to the particle moving out of focus and broadening of the STEM probe as it travels through more liquid before encountering the gold NP.

This raises the question whether it is possible to get a z coordinate for the particle simply by looking at the broadening of the imaged particle. Ideally, we would perform 3D ADF imaging by through-focal series analogous to Van Benthem and co-workers;[50] however, the NPs move too fast to use this procedure effectively. However, the blurring of the particles at various z heights within the cell may give us an indication of their positions. Blurring of the particles when moving in three dimensions happens via two ways.

First, if the particle is out of focus, it experiences a broader part of the probe instead of the most focussed part. The depth of focus δ_z depends on the semi-convergence angle α of the electron probe and can therefore be tuned depending on the range in z needed in the experiment. To estimate how big this effect would be for the 77 nm gold NPs we use[51]

$$\delta_z = \frac{d}{\alpha} \tag{4}$$

which yields $\delta_z = 7.7\,\mu\text{m}$ for our experimental conditions (d = 77 nm and α = 10 mrad). Since the particle can move at most 2 μm in the vertical direction, we assume that this is not the main effect leading to the blurring of the particles.

Second, the liquid, in this case glycerol, broadens the probe due to electron-solvent scattering, making the probe broader in the bottom of the cell. This effect can be calculated using[52]

$$d_{\text{blur}} = 1.2\times10^{3} T^{3/2} \frac{Z}{E}\sqrt{\frac{\rho}{W}} \tag{5}$$

where d_{blur} is the broadening of the electron probe, T is the thickness of the sample, Z is the average atomic number, W the average atomic weight, ρ the mass density, and E the energy of the electrons in eV. The beam broadening d_{blur} is plotted as a function of glycerol thickness in **Figure 8**a. For a thickness of 2 μm, we obtain d_{blur} = 26 nm, which is sufficient to explain the blurring of our particles at different heights in the liquid-cell.

To combine both effects, beam broadening and defocus conditions, we used CASINO to simulate the ADF-STEM images of a 77 nm gold NP at many different z heights in the liquid-cell. We then fitted the NP in the simulated image in the same way as for the experimental videos, using Trackpy. The FWHM of the fitted simulated particle at different z heights in the liquid-cell is shown in Figure 8b. The values of the FWHM for the experimental particles found in Movie S4, Supporting Information, are shown in Figure 8c. The experimentally found

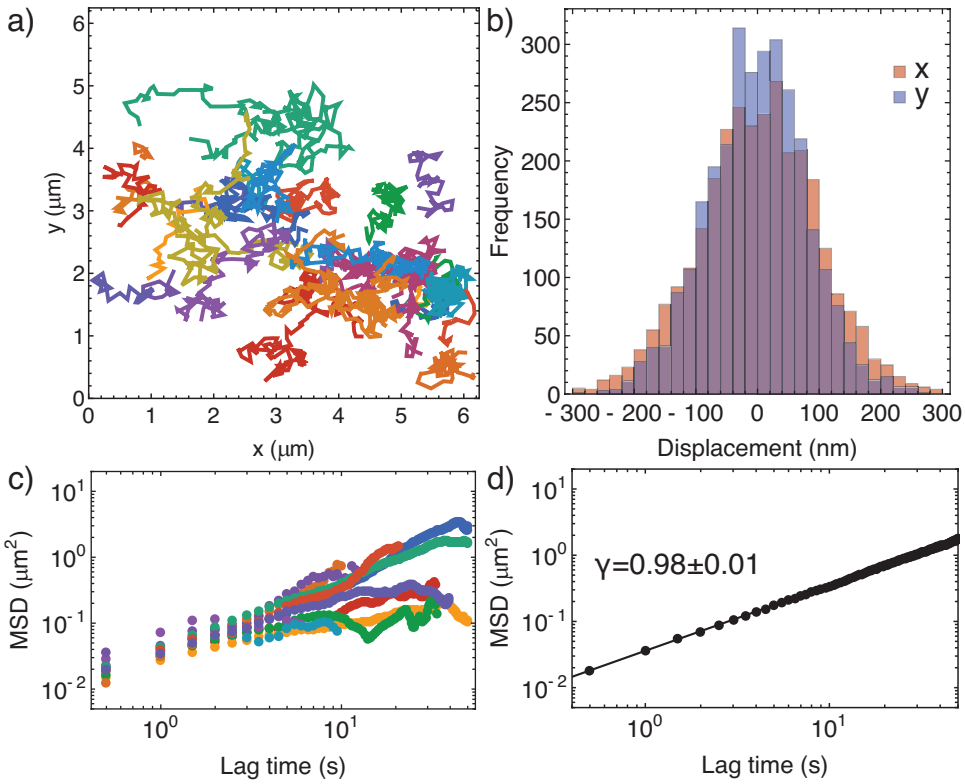

Figure 5. Analysis of diffusion of 77 nm gold NPs in the liquid-cell. a) First 30 tracks obtained from Movie S4, Supporting Information. b) Histogram of displacements between consecutive frames in the x- and y-directions. c) MSDs of 10 individual tracks obtained from Movie S4, Supporting Information. d) Ensemble averaged MSD from all individual MSDs in Movie S4, Supporting Information. The slope of the ensemble averaged MSD is 0.98 ± 0.01.

FWHMs go beyond those found in the simulations, which may be due to the liquid thickness being slightly larger than calculated. However, just as we would expect from the simulations, the histogram has a longer tail toward higher values of the FWHM, indicating that the FWHM increases more rapidly toward the lower parts of the liquid-cell. We therefore believe

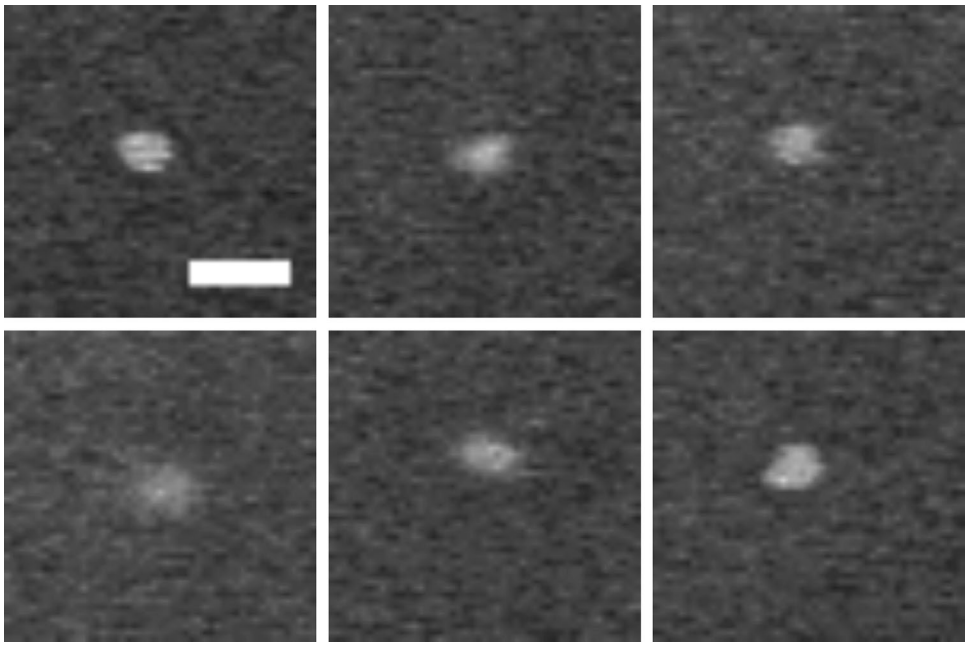

Figure 6. A single gold NP in the experimental Movie S4, Supporting Information, at t = 106, 132, 166, 188, 193, and 206 s. Due to its mobility in z, it becomes more or less blurry depending on the position in the cell. The scalebar indicates 200 nm.

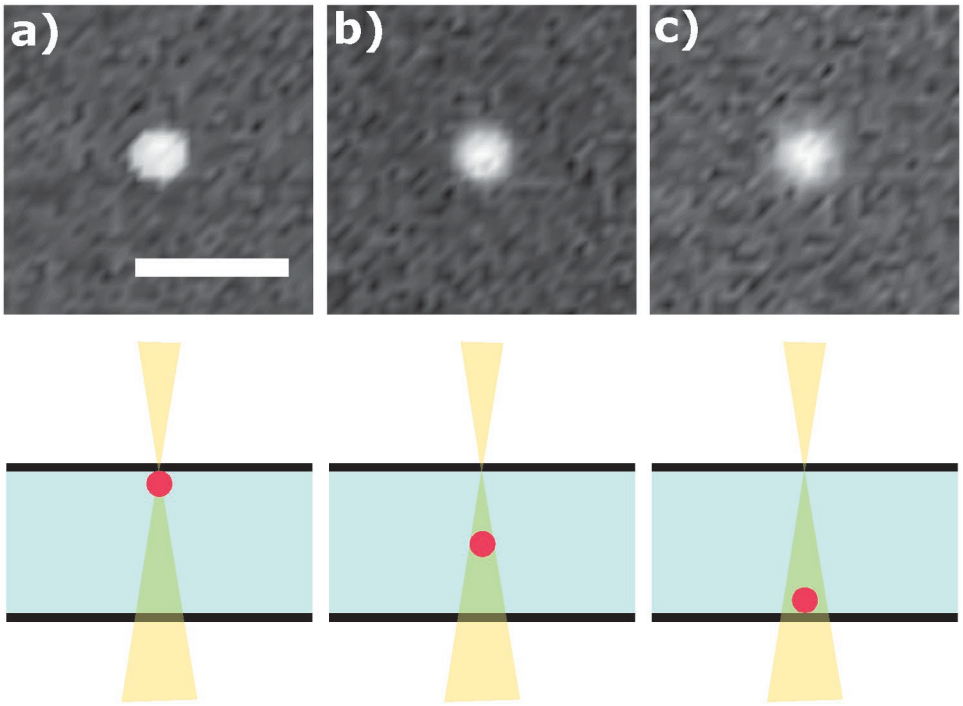

Figure 7. Simulated ADF-STEM images of a 77 nm gold NP using the software CASINO. The particles were put in different heights in the liquid-cell, namely a) on the top window, b) in the middle of the cell, and c) on the bottom window. The liquid thickness used was 2 micron. The input parameters for the Monte Carlo simulations were the same as used in the experiment for Movie S4, Supporting Information. The pixel size was 12.2 nm, the pixel dwell time was 1.9 µs and the electron dose rate was 9 e^{-} nm^{-2} s^{-1}. The focal point was on the top window and the semi-convergence angle α of the electron probe was 10 mrad. The scalebar is 200 nm.

that the simulations give a reasonable representation of the blurring of particles at different heights in the liquid-cell and that the blurring of the probe, d_{blur}, is sufficient to explain the blurring. Due to inherent noise at such low electron dose rates, however, we find that it is merely possible to provide a rough estimate of the particle position in z, rather than a precise coordinate. Also, the simulations show that in the top 1000 nm of the liquid-cell, the FWHM of particles should be roughly the same, as the blurring of the beam remains under 15% of the particle diameter in that region. Evidently, when the beam broadening exceeds 15% of the particle diameter, changes in the FWHM of the particle are noticeable. We do think using the broadening of the beam to infer z coordinates may be possible for smaller particles for similar liquid thicknesses.

As we did with the titania particles, we will consider the influence of the electron beam on the mobility of the gold NPs. We varied the electron dose rate via the strength of the condenser lens (Movies S3–S5, Supporting Information). **Table 1** shows no large difference in MSD analysis for different dose rates. However, we noticed that at an electron dose rate of 17 e^{-} nm^{-2} s^{-1} particles started to be repelled from the field of view (Movie S5, Supporting Information). As the particles are almost charge-neutral, phenomena related to charge are unlikely to explain this. However, the electric fields originating from beam–sample interactions must always be considered.[47] We calculated the temperature rise within the sample due to the electron probe (Supporting Information) and found it to be less than 1 K. However, we remark that a temperature gradient

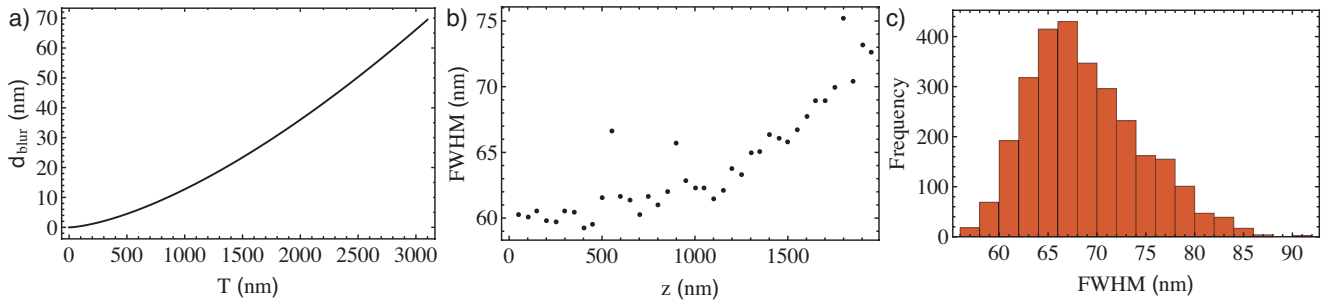

Figure 8. a) Beam broadening d_{blur} as calculated via Equation (5) as function of glycerol thickness. b) The FWHM of the 77 nm gold particle in simulated ADF-STEM images (see Figure 7) at various z heights inside the liquid-cell. The FWHM starts to increase when the beam is blurred sufficiently by the amount of liquid it has to travel through before it hits the particle. c) Histogram of experimental FWHM of all the single particles found in all frames in Movie S4, Supporting Information.

Table 1. Diffusion coefficient D and slope γ obtained from MSD analysis from videos of diffusing gold NPs at various dose rates.

Dose rate [$e^- nm^{-2} s^{-1}$]	D [$10^3 \mu m^2 s^{-1}$]	γ
0.6	8.0 ± 0.3	0.99 ± 0.04
1.6	8.1 ± 0.1	0.92 ± 0.01
3	11.0 ± 0.1	1.01 ± 0.01
9	8.8 ± 0.1	0.98 ± 0.01
17	7.8 ± 0.1	1.02 ± 0.01

of less than 1 K could be sufficient to explain why the particles start to leave the field of view via thermophoresis. Thermophoresis is the phenomenon where particles are driven toward the colder or warmer region of the liquid depending on the details of the particle-solvent interface.[53] A temperature difference of 1 K between the irradiated area and non-irradiated area could lead to a significant decrease in particle concentration in the irradiated region.[54–56] This thermophobic effect could lead the particles from the heated part of the irradiated region toward the colder region outside the field of view. However, the physical mechanisms are complex and not yet fully understood.[53]

At even higher electron dose rates, we observed that particles became stuck on the window. As the particles are charge-neutral, beam-induced charging effects may not be an important factor. It is more likely that at higher electron dose rates the PEG ligands on the surface of the NP may be affected. However, a definitive explanation can not be given at this time.

3. Conclusion

We conclude that 3D Brownian motion of NPs can be observed in LCSTEM under the right conditions, whereas previously only strongly hindered motion due to particle-window interactions was observed. Viscous solvents, GC and glycerol, helped slow down the particles, allowing them to be imaged within the time resolution of the available microscope system. These polar and viscous solvents, and especially a very low electron dose rate, helped mitigate electron beam effects normally leading to anomalous diffusion of particles in LC(S)TEM experiments. The obtained diffusion coefficients for both the negatively charged titania and the charge-neutral gold particles are close to those expected for free 3D single particle diffusion. No anomalous behavior was found for low electron dose rates as effects that could influence the motion such as electric fields and thermophoresis were suppressed. We thus conclude that observing Brownian motion of particles is indeed possible in a liquid-cell and we have identified the electron dose rate and possibly the dielectric constant of the medium as important design parameters for the experiments.

For future work on 3D motion of particles in LC(S)TEM, we think both the dielectric constant and the viscosity of the solvent should be carefully considered, along with a suppression of the electron dose rate and the imaging mode. STEM has a higher resolution in experiments with liquid thicknesses larger than approximately 100 nm,[36] provides a way of gauging the z positions of NPs as shown in this work, and likely causes less severe charging effects than TEM.[47] We therefore propose STEM as the preferred imaging mode.

We expect that, with the rapid improvements to EM detectors and sparse sampling approaches,[57] 3D Brownian motion experiments of much smaller particles will be possible in the near future. This makes it possible to conduct studies on NP interactions for NPs moving freely in solution, but also to study the (directed) self-assembly of NPs in real space and in real time using LC(S)TEM.[58]

4. Experimental Section

Liquid-Cell STEM: In order to image the NPs in the electron microscope, a liquid flow TEM holder with corresponding microchips (Hummingbird Scientific, USA) was used. The microchips had 50 nm thick amorphous silicon nitride (SiN_x) windows with a size of 50×200 μm. The spacer on one of the chips was 500 nm, but insertion in the microscope made the windows bulge outward, resulting in a thicker liquid layer. The two Si chips were glow-discharged for 2 min prior to the experiment in order to make their surfaces more hydrophilic. The microchip with spacer was then placed in a dedicated holder. A 1 μL L droplet of the dispersion was dropcasted onto the microchip. The second microchip was put onto the spacer chip with the hydrophilic side facing the opposite chip. The excess liquid was removed with filter paper. The liquid flow capability of the holder was not used. The used dispersions were titania particles dispersed in GC (4-(Hydroxymethyl)-1,3-dioxolan-2-one, Sigma-Aldrich 455067) and gold NPs dispersed in glycerol (Sigma-Aldrich CAS 56-81-5).

The liquid STEM experiments were carried out using a transmission electron microscope (Tecnai-F20, Thermo-Fischer Scientific), equipped with a field emission gun, and operating at 200 kV. The semi-convergence angle of the electron probe was 10 mrad. The annular dark-field (ADF) detector was used with a camera length of 120 mm. Image series were acquired with TEM imaging and analysis software (TIA). For the experiments with titania particles, the beam current measured via the fluorescent screen in vacuum was approximately 30 pA, while it was measured to be roughly 13 pA when the liquid-cell holder was inserted. A frame time of 0.2 s was used for most image series. The number of pixels was 256×256 or 512×512, which resulted in a pixel size of 17.5–49.5 nm depending on the magnification and amount of pixels. For the experiments with gold NPs, the beam current in vacuum ranged from 4 to 217 pA, depending on the spotsize. A frame time of 0.5 or 1 s was used. The number of pixels was 512×512 pixels, which resulted in a pixel size of 12 nm. The electron dose rate was calculated by using the screen current in vacuum and the total frame size. It is worthwhile to mention that in STEM, the value for the electron dose rate is not the only relevant entity. It is likely that the pixel dwell time and total frame time are also important parameters.[59] The liquid thickness was calculated via[15,52]

$$\frac{I_{\text{screen}}}{I_0} = \exp\left(-\left(\frac{t_{\text{SiN}_x}}{I_{\text{SiN}_x}} + \frac{t_{\text{liquid}}}{I_{\text{liquid}}}\right)\right) \tag{6}$$

Particle Tracking: The positions of the titania particles in each frame were tracked using the ImageJ plugin MTrackJ.[37] The position for a particle was determined manually for each frame. The tracking error for the particles of 350 nm diameter, determined by tracking a particle that was stuck on the window, was 13 ± 4 nm. The positions of the gold NPs were determined using Trackpy, based on the feature-finding and linking algorithms of Crocker & Grier.[60] No drift was observed and no drift correction was applied for all videos.

Monte Carlo Simulations Using CASINO: To simulate ADF-STEM images the CASINO software was used.[43–45] The used physics model for the total and partial cross sections in the simulation software

was that of an empirical analytical fit to the Mott cross sections by Browning et al.[61] The specific parameters of the sample and the electron probe were taken to be as close to the experimental parameters as possible.

For the 350 nm titania particle in GC, a layer of 2.3 μm of glycerol carbonate was put between two 50 nm thick Si_3N_4 windows. A 350 nm titania particle was positioned at various heights within the glycerol carbonate layer. The electron probe was set to have a semi-convergence angle of 10 mrad and a diameter of 1 nm. The beam distribution was Gaussian. The electron probe had an energy of 200 keV and had its focal point on the top window minus one particle radius. The pixel size was 17.5 nm and the number of simulated electrons per pixel N was 375, as calculated from the beam current I and the pixel dwell time τ via

$$N = \frac{I \times \tau}{e} \tag{7}$$

where e is the electron charge. The ADF detector with a quantum efficiency of 100% was set to have a minimum and maximum semi-angle of 33 and 450 mrad, respectively.

For the 77 nm gold NP in glycerol, a layer of 2 μm of glycerol was between two 50 nm thick Si_3N_4 windows. A 77 nm gold NP was positioned at various heights within the glycerol layer. The electron probe was set to have a semi-convergence angle of 10 mrad and a diameter of 1 nm. The beam distribution was Gaussian. The electron probe had an energy of 200 keV and had its focal point on the top window minus one particle radius. The pixel size was 12.2 nm and the number of simulated electrons per pixel N was 663. The ADF detector with a quantum efficiency of 100% was set to have a minimum and maximum semi-angle of 33 and 450 mrad, respectively.

Supporting Information

Supporting Information is available from the Wiley Online Library or from the author.

Acknowledgements

The authors thank Fabian Hagemans for the measurement of the viscosity of glycerol carbonate. This project received funding from the European Research Council (ERC) via the ERC Consolidator Grant NANO-INSITU (grant no. 683076). The authors also acknowledge funding from the NWO-TTW Perspectief Program "Understanding Processes Using Operando Nanoscopy," project UPON-B3 (no. 14206). M.B. acknowledges funding from the Netherlands Center for Multiscale Catalytic Energy Conversion (MCEC), an NWO Gravitation programme funded by the Ministry of Education, Culture, and Science of the government of the Netherlands.

Conflict of Interest

The authors declare no conflict of interest.

Keywords

3D motion, liquid-cell electron microscopy, nanoparticles, particle diffusion

Received: December 30, 2019
Revised: March 27, 2020
Published online: May 6, 2020

[1] B. D. Leahy, N. Y. C. Lin, I. Cohen, *Curr. Opin. Colloid Interface Sci.* **2018**, *34*, 32.
[2] M. C. Jenkins, S. U. Egelhaaf, *Adv. Colloid Interface Sci.* **2008**, *136*, 65.
[3] M. A. Bevan, S. L. Eichmann, *Curr. Opin. Colloid Interface Sci.* **2011**, *16*, 149.
[4] N. De Jonge, F. M. Ross, *Nat. Nanotechnol.* **2011**, *103*, 163.
[5] F. M. Ross, *Science* **2015**, *350*, aaa9886.
[6] S. W. Chee, Z. Baraissov, N. D. Loh, P. T. Matsudaira, U. Mirsaidov, *J. Phys. Chem. C* **2016**, *120*, 20462.
[7] P. Alivisatos, Q. Chen, J. Smith, J. Park, K. Kim, D. Ho, H. Rasool, A. Zettl, *Nano Lett.* **2013**, *13*, 4556.
[8] J. Liu, Z. Wang, A. Sheng, F. Liu, F. Qin, Z. L. Wang, *Environ. Sci. Technol.* **2016**, *50*, 5606.
[9] Y. Liu, X. M. Lin, Y. Sun, T. Rajh, *J. Am. Chem. Soc.* **2013**, *135*, 3764.
[10] J. Lu, Z. Aabdin, N. D. Loh, D. Bhattacharya, U. Mirsaidov, *Nano Lett.* **2014**, *14*, 2111.
[11] L. R. Parent, E. Bakalis, A. Ramírez-Hernández, J. K. Kammeyer, C. Park, J. De Pablo, F. Zerbetto, J. P. Patterson, N. C. Gianneschi, *J. Am. Chem. Soc.* **2017**, *139*, 17140.
[12] A. S. Powers, H. G. Liao, S. N. Raja, N. D. Bronstein, A. P. Alivisatos, H. Zheng, *Nano Lett.* **2017**, *17*, 15.
[13] M. T. Proetto, A. M. Rush, M. P. Chien, P. Abellan Baeza, J. P. Patterson, M. P. Thompson, N. H. Olson, C. E. Moore, A. L. Rheingold, C. Andolina, J. Millstone, S. B. Howell, N. D. Browning, J. E. Evans, N. C. Gianneschi, *J. Am. Chem. Soc.* **2014**, *136*, 1162.
[14] E. A. Ring, N. de Jonge, *Micron* **2012**, *43*, 1078.
[15] A. Verch, M. Pfaff, N. De Jonge, *Langmuir* **2015**, *31*, 6956.
[16] E. R. White, M. Mecklenburg, B. Shevitski, S. B. Singer, B. C. Regan, *Langmuir* **2012**, *28*, 3695.
[17] T. J. Woehl, K. L. Jungjohann, J. E. Evans, I. Arslan, W. D. Ristenpart, N. D. Browning, *Ultramicroscopy* **2013**, *127*, 53.
[18] T. J. Woehl, T. Prozorov, *J. Phys. Chem. C* **2015**, *119*, 21261.
[19] H. Zheng, S. A. Claridge, A. M. Minor, A. P. Alivisatos, U. Dahmen, *Nano Lett.* **2009**, *9*, 2460.
[20] G. Lin, S. W. Chee, S. Raj, P. Král, U. Mirsaidov, *ACS Nano* **2016**, *10*, 7443.
[21] G. Lin, X. Zhu, U. Anand, Q. Liu, J. Lu, Z. Aabdin, H. Su, U. Mirsaidov, *Nano Lett.* **2016**, *16*, 1092.
[22] E. Sutter, *Nat. Commun.* **2016**, *7*, 11213.
[23] S. F. Tan, U. Anand, U. Mirsaidov, *ACS Nano* **2017**, *11*, 1633.
[24] S. F. Tan, S. W. Chee, G. Lin, U. Mirsaidov, *Acc. Chem. Res.* **2017**, *50*, 1303.
[25] X. Tian, H. Zheng, U. Mirsaidov, *Nanoscale* **2017**, *9*, 10044.
[26] G. Zhu, Y. Jiang, W. Huang, H. Zhang, F. Lin, C. Jin, *Chem. Commun.* **2013**, *49*, 10944.
[27] J. Kim, Z. Ou, M. R. Jones, X. Song, Q. Chen, *Nat. Commun.* **2017**, *8*, 761.
[28] M. Piffoux, N. Ahmad, J. Nelayah, C. Wilhelm, A. Silva, F. Gazeau, D. Alloyeau, *Nanoscale* **2018**, *10*, 1234.
[29] D. J. Kelly, M. Zhou, N. Clark, M. J. Hamer, E. A. Lewis, A. M. Rakowski, S. J. Haigh, R. V. Gorbachev, *Nano Lett.* **2018**, *18*, 1168.
[30] M. A. Boles, M. Engel, D. V. Talapin, *Chem. Rev.* **2016**, *116*, 11220.
[31] E. Mine, M. Hirose, D. Nagao, Y. Kobayashi, M. Konno, *J. Colloid Interface Sci.* **2005**, *291*, 162.
[32] Y. Chernyak, *J. Chem. Eng. Data* **2006**, *51*, 416.
[33] N. Jiang, *Micron* **2016**, *83*, 79.
[34] G. Ou, B. He, X. Li, J. Lei, *Sci. World J.* **2012**, *2012*, 697161.
[35] J. Wang, T. Yong, J. Yang, C. Ouyang, L. Zhang, *RSC Adv.* **2015**, *5*, 17660.
[36] N. de Jonge, *Ultramicroscopy* **2018**, *187*, 113.
[37] E. Meijering, O. Dzyubachyk, I. Smal, *Methods for Cell and Particle Tracking*, 1st ed., Elsevier, New York **2012**.
[38] H. Qian, M. P. Sheetz, E. L. Elson, *Biophys. J.* **1991**, *60*, 910.

[39] M. J. Saxton, *Biophys. J.* **1997**, *72*, 1744.
[40] X. Michalet, *Phys. Rev. E: Stat., Nonlinear, Soft Matter Phys.* **2010**, *82*, 041914.
[41] L. R. Parent, E. Bakalis, M. Proetto, Y. Li, C. Park, F. Zerbetto, N. C. Gianneschi, *Acc. Chem. Res.* **2018**, *51*, 3.
[42] J. De Graaf, T. Peter, L. P. Fischer, C. Holm, *J. Chem. Phys.* **2015**, *143*, 084108.
[43] D. Drouin, A. R. Couture, D. Joly, X. Tastet, V. Aimez, R. Gauvin, *Scanning* **2007**, *29*, 92.
[44] H. Demers, N. Poirier-Demers, A. R. Couture, D. Joly, M. Guilmain, N. De Jonge, D. Drouin, *Scanning* **2011**, *33*, 135.
[45] N. Poirier-Demers, H. Demers, D. Drouin, N. de Jonge, *Microsc. Microanal.* **2011**, *17*, 980.
[46] N. M. Schneider, M. M. Norton, B. J. Mendel, J. M. Grogan, F. M. Ross, H. H. Bau, *J. Phys. Chem. C* **2014**, *118*, 22373.
[47] N. Jiang, *Ultramicroscopy* **2017**, *179*, 81.
[48] N. Jiang, *J. Phys. D: Appl. Phys.* **2013**, *46*, 305502.
[49] C. Hanske, G. González-Rubio, C. Hamon, P. Formentín, E. Modin, A. Chuvilin, A. Guerrero-Martínez, L. F. Marsal, L. M. Liz-Marzán, *J. Phys. Chem. C* **2017**, *121*, 10899.
[50] K. van Benthem, A. R. Lupini, M. P. Oxley, S. D. Findlay, L. J. Allen, S. J. Pennycook, *Ultramicroscopy* **2006**, *106*, 1062.
[51] N. de Jonge, R. Sougrat, B. M. Northan, S. J. Pennycook, *Microsc. Microanal.* **2010**, *16*, 54.
[52] N. de Jonge, N. Poirier-Demers, H. Demers, D. B. Peckys, D. Drouin, *Ultramicroscopy* **2010**, *110*, 1114.
[53] R. Piazza, A. Parola, *J. Phys.: Condens. Matter* **2008**, *20*, 153102.
[54] S. Duhr, D. Braun, *Phys. Rev. Lett.* **2006**, *96*, 168301.
[55] Y. Zhao, C. Zhao, J. He, Y. Zhou, C. Yang, *Soft Matter* **2013**, *9*, 7726.
[56] E. L. Talbot, J. Kotar, L. Parolini, L. Di Michele, P. Cicuta, *Nat. Commun.* **2017**, *8*, 15351.
[57] L. Kovarik, A. Stevens, A. Liyu, N. D. Browning, *Appl. Phys. Lett.* **2016**, *109*, 164102.
[58] Z. Ou, Z. Wang, B. Luo, E. Luijten, Q. Chen, *Nat. Maters.* **2019**, *19*, 450.
[59] P. Abellan, T. J. Woehl, L. R. Parent, N. D. Browning, J. E. Evans, I. Arslan, *Chem. Commun.* **2014**, *50*, 4873.
[60] J. C. Crocker, D. G. Grier, *J. Colloid Interface Sci.* **1996**, *310*, 298.
[61] R. Browning, T. Z. Li, B. Chui, J. Ye, R. F. Pease, Z. Czyzewski, D. C. Joy, *J. Appl. Phys.* **1994**, *76*, 2016.